Combining 3D geological modelling techniques to address variations in geology, data type and density – An example fro....

Article *in* Computers & Geosciences · April 2015

DOI: 10.1016/j.cageo.2015.04.010

CITATIONS
11

READS
173

5 authors, including:

Flemming Jørgensen
Geological Survey of Denmark and Greenland
92 PUBLICATIONS **1,358** CITATIONS
SEE PROFILE

Anne-Sophie Høyer
Geological Survey of Denmark and Greenland
22 PUBLICATIONS **125** CITATIONS
SEE PROFILE

Peter B. E. Sandersen
Geological Survey of Denmark and Greenland
46 PUBLICATIONS **637** CITATIONS
SEE PROFILE

Xiulan He
University of Copenhagen
7 PUBLICATIONS **36** CITATIONS
SEE PROFILE

Computers & Geosciences 81 (2015) 53–63

Contents lists available at ScienceDirect

Computers & Geosciences

journal homepage: www.elsevier.com/locate/cageo

Short note

Combining 3D geological modelling techniques to address variations in geology, data type and density – An example from Southern Denmark

Flemming Jørgensen [a,*], Anne-Sophie Høyer [a], Peter B.E. Sandersen [a], Xiulan He [b], Nikolaj Foged [c]

[a] Geological Survey of Denmark and Greenland – GEUS, Lyseng Alle 1, DK-8270 Højbjerg, Denmark
[b] COWI A/S, Parallelvej 2, DK-2800 Kongens Lyngby, Denmark
[c] Department of Geoscience, Aarhus University, C. F. Møllers Alle 4, DK-8000 Aarhus, Denmark

ARTICLE INFO

Article history:
Received 12 March 2015
Received in revised form
26 April 2015
Accepted 27 April 2015
Available online 30 April 2015

Keywords:
3D geological modelling
AEM data
Cognitive layer modelling
Multi-Point Simulation
Clay fraction modelling
Voxel model

ABSTRACT

The very complex near-surface geology in Denmark is a big challenge when constructing 3D geological models. Borehole data alone are normally insufficient for proper 3D modelling because data are too widespread. Therefore, Airborne ElectroMagnetic (AEM) techniques are often used to obtain supplementary information on the spatial distribution and composition of the geology.

A large-scale AEM survey and high-resolution seismic data along with both new and existing borehole data and seismic data from hydrocarbon exploration were available for the construction of a detailed 3D geological model in our study area. The data are unevenly distributed, and only part of the study area was covered by the AEM survey. Cross-cutting tunnel valleys, erosional unconformities, delta units and a large glaciotectonic complex are among the geological features identified in the area. The geological complexity varies significantly across the model area.

A broad geological overview and understanding of the area was obtained by joint cognitive interpretation of the geophysical and the geological data. To address the geological complexity and the very high level of detail gained from the AEM data, the model was constructed as a voxel model with lithofacies attributes supplemented by a number of bounding surfaces. In areas where the geology is not too detailed and complex, the model was constructed manually, whereas automated methods were used to populate voxels in areas with a high complexity. The automated methods comprised clay fraction modelling, which was used where AEM data are available, and stochastic modelling, which was used outside the area covered by AEM data.

Our study shows that it is advantageous to combine several modelling methods in areas with varying geological complexity and data density. The choice of modelling methods should depend on the character and coverage of available data and on variations in geology throughout the model area.

1. Introduction

3D geological modelling is a rapidly expanding discipline as demand for knowledge about the structure and composition of the subsurface is increasing. Additionally, this growth is facilitated by developments in computer technology and software (Berg et al., 2011), and also by considerable ongoing improvements in subsurface geophysical mapping methods (Schamper et al., 2014a, 2014b; Steuer et al., 2009). Advances in computer technology and software development allow us to construct and visualise detailed and increasingly complex models with ease, but do not necessarily produce more credible models. To enhance the credibility of our models, data that characterise the subsurface sufficiently in three dimensions are needed, especially when the geology is spatially complex and layers and layer boundaries are difficult or impossible to correlate between boreholes.

3D geological models are traditionally created as framework models or pseudo-3D models in which a number of 2D cross sections are made across the model area, either through selected boreholes or with boreholes transferred onto to the profiles within a given buffer zone. Stratigraphical interpretations are then inserted on the sections by correlation between the boreholes and fitted to other cross sections where they intersect (Kessler et al., 2009; Royse, 2010; Wycisk et al., 2009). Finally, surfaces are interpolated between the sections. This approach is based on iterative, manual and cognitive interpretation along cross sections. The geologist makes use of background knowledge about geology and geological processes in the modelling process. This results in a

* Corresponding author. Fax: +45 38142050.
E-mail address: flj@geus.dk (F. Jørgensen).

http://dx.doi.org/10.1016/j.cageo.2015.04.010
0098-3004/

subjective model, but the model fully facilitates the use of all available information – depending, of course, on the geologist's skills.

In recent years, Airborne ElectroMagnetic (AEM) data have increasingly proven to be successful in the delivery of spatially dense data by providing detailed 3D information of geological structures and layers (Schamper et al., 2014b). Although geological structures and layers need to be of a considerable size to be resolved and even though a significant resistivity contrast needs to exist between the units (Jørgensen et al., 2013), such data can often considerably improve the basis for reliable 3D geological models (Høyer et al., 2015; Jørgensen et al., 2013; Klimke et al., 2013).

Data sets from dense AEM surveys sets challenge traditional manual modelling because the amount of information provided by such data is huge and difficult to summarise and employ. The data have to be aggregated and interpolated before use, and new approaches and tools need to be developed (Jørgensen et al., 2013). One way of handling the overwhelming amount of data is to use stochastic methods in the modelling phase. Stochastic methods include transition probability indicator simulation (Carle and Fogg, 1996), Multi-Point Simulation methods (MPS) (Daly and Caers, 2010; Strebelle, 2002) and sequential indicator simulation (Deutsch and Journel, 1998). Only relatively few attempts to apply AEM data in stochastic modelling have so far been documented. He et al. (2013) used AEM data as training image in an MPS model, and He et al. (2014a) and Koch et al. (2014) used AEM data for soft conditioning in transition indicator probability simulations, whereas Gunnink et al. (2012) and Gunnink and Siemon (2014) used other stochastic tools. The stochastic modelling methods provide a set of equally plausible models depending on the given assumptions and conditions.

Another automated method recently developed is the Clay Fraction (CF) modelling concept (Foged et al., 2014). The CF model concept is a further development of the Accumulated Clay Thickness (ACT) concept (Christiansen et al., 2014). By this approach, the clay fraction is calculated through inversion of both borehole data and AEM resistivity models and populated into a voxel model. Common for the automated methods is that they are normally restricted to providing only a few model properties, typically sand and clay.

The various methodologies for 3D geological modelling have different advantages and drawbacks, depending mainly on available data (e.g. type and density) and geology (e.g. property and heterogeneity). Combined use of different methodologies is therefore ideal in various situations (Raiber et al., 2012; Royse, 2010; Sharpe et al., 2007; Stafleu et al., 2011; Venteris, 2007). In this paper, we present a 3D geological model that combines three different modelling methodologies, each selected to provide the best possible outcome in sub-volumes of the model. We show how the choice of methodology should optimally be a product of differences in the data types available, the data density and the geological complexity.

2. The model area and purpose

The model area is situated just north of the Danish-German border in the south-western part of the Jutland peninsula (Fig. 1). It is about 33 km in E–W direction and 30 km in N–S direction giving a total area of 625 km^2. It is a rather flat area composed by a number of glacially formed “hill-islands” which are partly covered by a thin sheet of outwash sediments forming a large outwash plain with a gentle dip towards the west. A flat Holocene marshland is found in the south-western part of the area. The area reaches a maximum elevation of 62 m above sea level in the northern part.

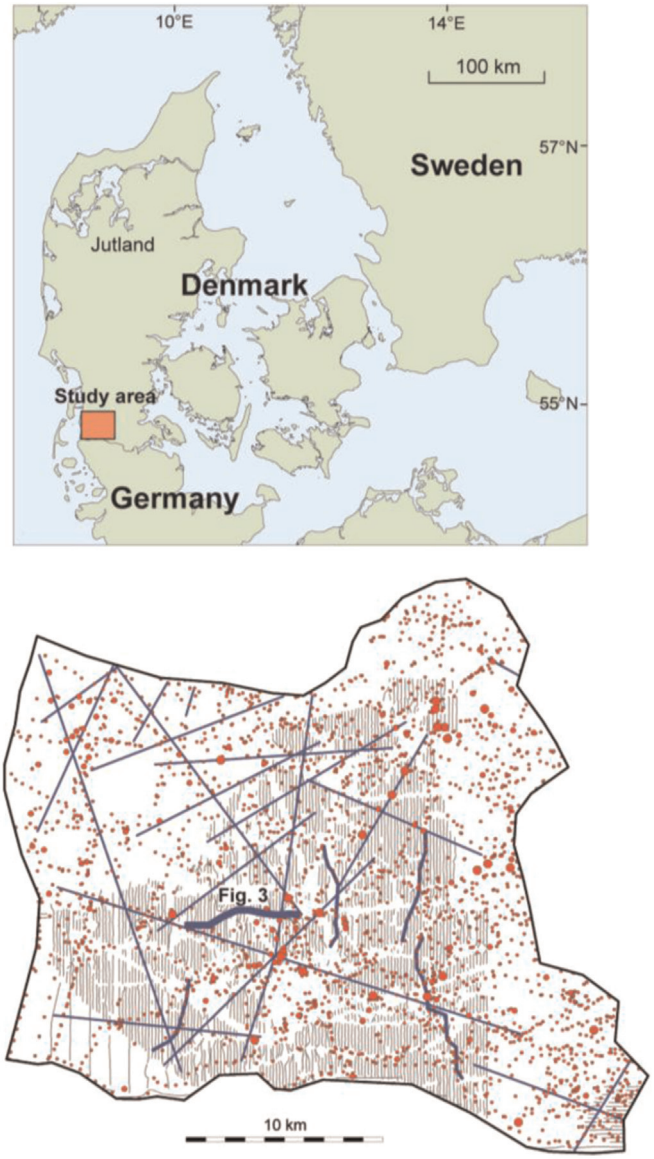

Fig. 1. Upper: overview map. Lower: map of study area and data. The straight blue lines are conventional seismic data; curved blue lines are high-resolution seismic sections. The thick curved blue line is the high-resolution seismic section shown in Fig. 3. Large red dots are deep boreholes; small red dots are shallow boreholes; grey lines/dots are SkyTEM flight lines/soundings. (For interpretation of the references to colour in this figure legend, the reader is referred to the web version of this article.)

The model was basically constructed to provide input for numerical groundwater flow modelling. After geological model construction, the model was therefore further developed and designed for hydrological purposes, but this part of the modelling project is not presented herein.

3. Data and data handling

The geophysical methods, handling of data and the surveys performed in the area are described in detail in Jørgensen et al. (2012). Below, we only provide a short summary focussing on the methodologies that are important for the 3D geological modelling.

3.1. Airborne electromagnetics

The airborne survey is performed by the helicopter-borne electromagnetic time-domain SkyTEM system (Sørensen and Auken, 2004). When the collected data are processed and inverted (Viezzoli et al., 2009), each single sounding estimates the electrical resistivity down to a depth of 250–300 m. The survey includes 1750 line km with an average flight line spacing of 166 m. The survey does not cover the entire model area, only about 325 km^2 (Fig. 1). The lateral resolution along the flight lines is about 25–30 m in the uppermost part of the section and decreases significantly to more than 100–200 in the deeper part. The vertical resolution also decreases considerably with depth. The SkyTEM resistivity data are interpolated and converted into a 3D resistivity grid, which can be sliced horizontally and vertically to ease comparison with other data.

3.2. Seismic data

Five high-resolution seismic reflection profiles covering a total distance of 29.5 km were recorded in 2010 (Fig. 1), using an IVI Minivib T7000 3.5-ton vibrator and 224 towed geophones (Rambøll, 2010). This system setup is capable of resolving the subsurface at depths from about 20 m to 700 m.

For the modelling, all available conventional oil seismic data are also used. Such seismic sections frequently cross the model area (Fig. 1), but most have no or only a very poor resolution in the relevant part of the subsurface ($<$ 500–700 m). Some of the seismic sections show decent resolution from about 50–100 m and down. These few, good oil seismic lines provide valuable information about the deeper subsurface, where the data density is otherwise very low.

3.3. Borehole data

The borehole data are extracted from the Danish national borehole database (http://jupiter.geus.dk) and comprise about 3200 boreholes in the model area. The borehole data were automatically classified into five quality-rating groups using a series of dedicated database queries. The aim of the borehole rating is to identify boreholes from which correct and detailed lithological information can be derived and to determine which boreholes should be used with caution or be discarded before further use. The quality rating result is actively used as a part of the modelling process by assigning quality weights to the groups. The rating focuses on the capability of the borehole data to distinguish between clay and sand and to define layer boundaries in between these sediment classifications.

The rating system is based on six main criteria: (1) accuracy of the geographical position of the boreholes, (2) drilling method and purpose, (3) credibility of driller, (4) soil sample frequency per metre drilled, (5) age of borehole, (6) occurrence of contradicting and erroneous information related to, for instance, borehole elevation, position, drilling methods, etc. Finally, rating scores for each borehole are calculated according to weighted impacts from each criterion. All boreholes are thereby divided into the five rating groups, with group 1 referring to the most trusted boreholes having the highest quality and group 5 referring to the boreholes of the lowest quality.

A total of 30% of the boreholes were found to be of good or a reasonably good quality (rating groups 1 and 2), 32% were found to have below medium to poor quality with only minor amounts of information (rating groups 3 and 4), and 12% of the boreholes were considered useless and were discarded from the data set (rating group 5).

Two new investigatory drillings have recently been performed in the area. These new drillings reach depths of 325 m (Jupiter file no. 167.1545) and 358 m (Jupiter file no. 167.1538). They have been sampled and described in detail and wireline logged with resistivity tools (Orbicon, 2010, 2011).

4. Conceptual geological model

Previous knowledge from the area has primarily been based on the borehole data and the conventional seismic data. Above the limestone situated at depths of more than 500–600 m, the Tertiary and Quaternary successions can generally be split into three main sedimentary units: (1) very fine-grained hemipelagic clays of the Palaeogene (Friborg and Thomsen, 1999), then (2) a package of clay, sand and silt layers from the Miocene (Rasmussen et al., 2010) and (3) on top a cover of Pleistocene sediments. Based on the fact that borehole data often show big lateral variations in the geology over short distances and supported by observations from old seismic data and gravity data, it has been described that these three major sedimentary units were cut by faults (Friborg and Thomsen, 1999), eroded by deep buried tunnel valleys (Friborg and Thomsen, 1999; Jørgensen and Sandersen, 2006; Thomsen, 1991) and deformed by glaciotectonics (Andersen, 2004; Friborg, 1989). It has not previously been possible to map in detail the position and distribution of these elements and the major sedimentary units.

The new data confirm previous knowledge and add much new detailed knowledge, especially about the geological architecture. Interpretations of the data (Figs. 3 and 4) were presented in Jørgensen et al. (2012), so only a short review is given here. The interpreted geology of the area is conceptualised in the stratigraphical log shown in Fig. 2.

In the majority of the study area, the surface of the Palaeogene clay is situated too deep to be detected by the SkyTEM data ($>$ 300 m). In smaller areas, however, the Palaeogene is revealed as a layer with very low resistivity. The indications of Palaeogene clay in the resistivity data briefly fit with the new deep boreholes in the area and with a strong reflector that can be followed over most of the area in both the high-resolution and the conventional seismic data. A deep-seated graben structure, the Tønder Graben, crosses the area from southeast to northwest. The structure is

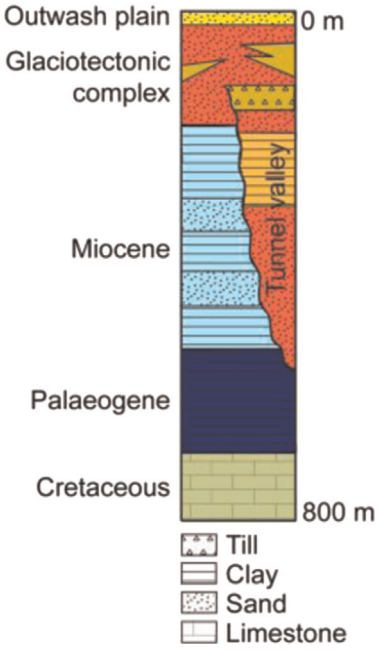

Fig. 2. Conceptual stratigraphical log (modified after from Jørgensen et al. (2012)).

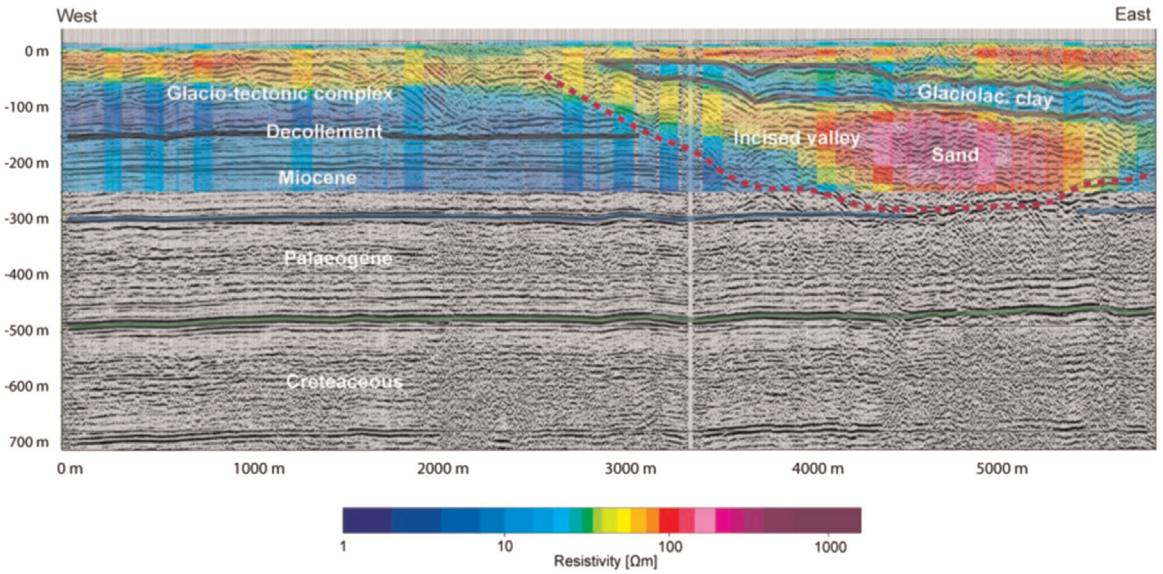

Fig. 3. One of the high-resolution seismic profiles together with the SkyTEM resistivity grid. For location, see Fig. 1. Geological interpretations are drawn and noted on the profile. Broken line in red shows the erosional boundary of the tunnel valley. Modified after Jørgensen et al. (2012). (For interpretation of the references to colour in this figure legend, the reader is referred to the web version of this article.)

bounded by faults and/or flexures that are visible in both SkyTEM data (Fig. 4) and seismic data. The Miocene succession above has been thoroughly studied in deep boreholes and in the seismic data, and a sequence stratigraphical model has been developed for large parts of the neighbouring areas (Rasmussen et al., 2010). In the present study, this was extended to cover the model area. The Miocene is composed by the sandy deltaic Bastrup Formation, the clayey marine Klintinghoved formation, the more silty Arnum formation and the sandy Odderup formation. The marine clay formations are occasionally intervened by sandy delta lobes. The top of the Miocene is characterised by the clay-rich Måde Group.

The buried valleys comprise at least three different cross-cutting generations. They cut deeply into the Miocene, and the deepest valley is up to 470 m deep. The valleys have undulating floors and are typically 1–3 km wide. The valleys are filled with glacial deposits, typically thick layers of glaciofluvial origin, comprising both fine-grained and coarse-grained material. The valleys are seen as erosional structures on the seismic data (Fig. 3) and often as longitudinal features on some horizontal slices through the SkyTEM resistivity grid (Fig. 4). Except for a widespread cover of outwash deposits and Holocene sediments, the upper parts of the subsurface are generally deformed by glaciotectonics producing very complex thrusted and folded layers of Miocene and glacial origin. These glaciotectonic complex structures can be seen in the seismic data as well as in the SkyTEM data. As in the Ølgod area not far away (Høyer et al., 2013a), a decollement plane with associated thrust sheets and folds reveal a glaciotectonic origin (Fig. 4). The glaciotectonically deformed features are evident in the SkyTEM data as arc-shaped southeast–northwest oriented low-resistive features on the resistivity map in Fig. 4. Thus, the extent and thickness of the glaciotectonic complex are mapped through combined use of the seismic data and the SkyTEM data. The depth to which the sediments are heavily deformed extends down to between 40 and 150 m below sea level.

The covering outwash unit is undisturbed by glaciotectonics and composed by outwash sand with a maximum thickness of about 40 m. The outwash unit is seen as a thin resistive layer in the SkyTEM data. Finally, the very thin (less than 12 m) Holocene sediments are only seen in the borehole data. Occurrence of saltwater in marshland in the south-western part of the area disturbs the mapping results by blurring the general picture with very low resistivities (Fig. 4).

5. Modelling methodologies used

For the overall model construction, we used the software package GeoScene3D (GeoScene3D, 2014, http://www.geoscene3d.com). This software facilitates visualisation of data in cross sections, horizontal sections, map views and in 3D view. The software can handle the construction of both framework models and voxel models.

The geological modelling techniques used in our model comprise CF modelling, MPS modelling and cognitive layer modelling. These are briefly described in the following:

5.1. CF modelling

The CF modelling method has been developed to create an automated method for 3D modelling of the subsurface in large areas with both resistivity data and borehole data (Foged et al., 2014). The model output is expressed as a clay fraction, which refers to the relative clay content in a voxel regardless of the clay type. The input data are derived from lithological borehole logs, which are divided into a binary scheme of 'clay sediments' (clay till, meltwater clay, Palaeogene clay, etc.) and 'non-clay sediments' (meltwater sand, meltwater gravel, Miocene sand, etc.). Fundamentally, the concept combines resistivity and borehole information through inversion to establish the optimum translator function between the resistivity and clay fraction, while allowing spatial variations in this translation. The translator function holds an upper threshold value for clay (CF=1) and a lower threshold value for non-clay (CF=0). For resistivities between the thresholds, the translator function returns CF-values between 0 and 1 (Christiansen et al., 2014; Foged et al., 2014). The quality rating of each borehole is taken into account, so that the most trustworthy boreholes are assigned the highest weight in the determination of the translator function. Finally, the optimised translator function is applied to the resistivity models to obtain a 3D clay fraction model.

5.2. MPS modelling

Stochastic modelling is performed by multi-point geostatistics (MPS) (Strebelle, 2002) and applied with the Stanford Geostatistical Modelling Software (SGeMS) software (Remy et al., 2009). To

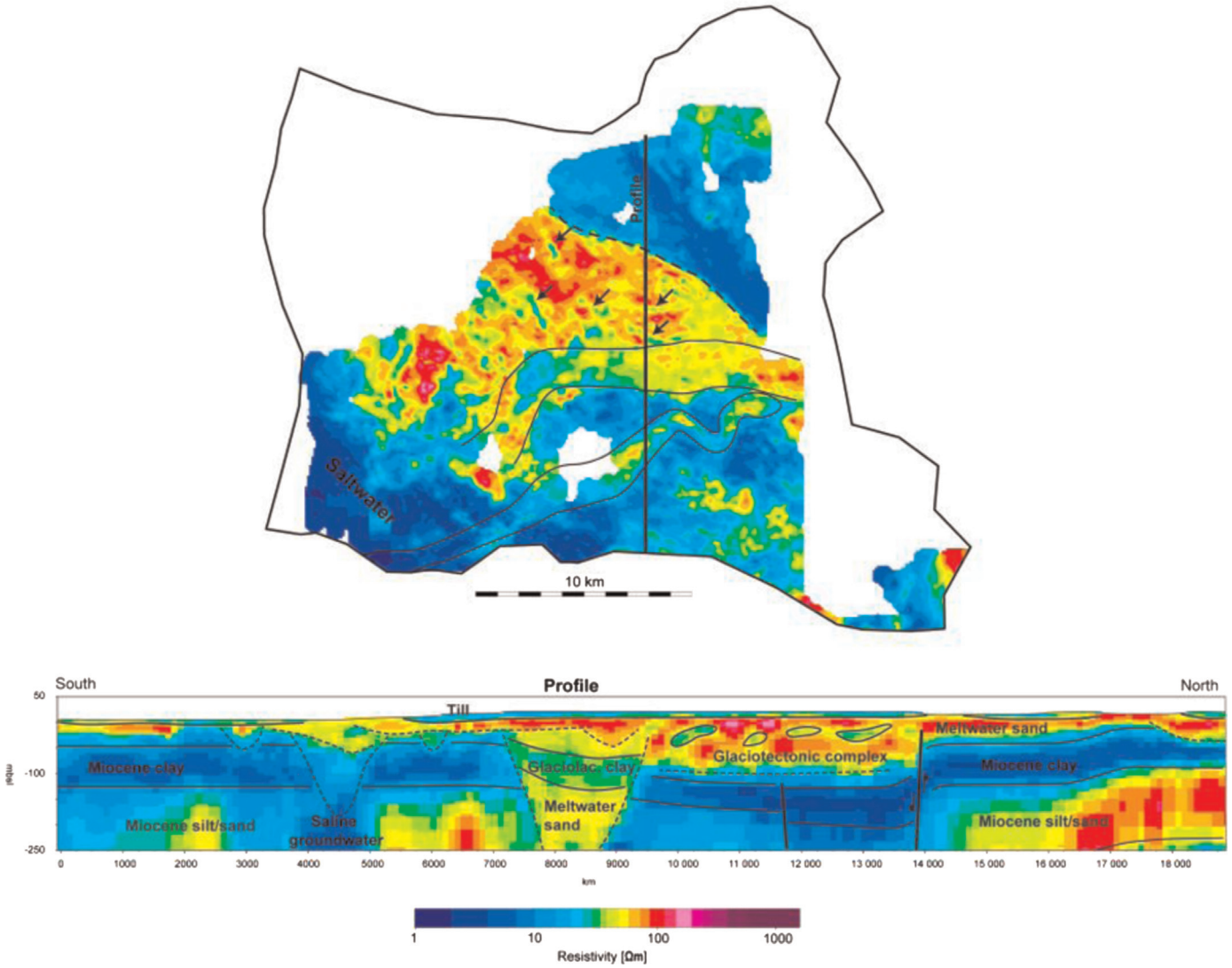

Fig. 4. SkyTEM resistivity grid shown in map and profile view. The map view shows a horizontal slice at 47.5 m below sea level. The location of the profile is drawn on the map. Geological interpretations are outlined on the profile. The broken line on the map represents the northern fault along the graben structure; unbroken lines outline a couple of buried valleys identical with the ones marked with arrows in Fig. 8. Arrows in Fig. 4 point at thrust structures within the glaciotectonic complex. Modified from Jørgensen et al. (2012).

create MPS simulations, we used the "SNESIM" (Single Normal Equation SIMulation) algorithm, which is an advanced pixel-based approach that picks the probability distribution directly from a pre-defined training image. In the present study, we used a binary system consisting of clay and sand only and the binary borehole information was therefore used as input in the simulations. The borehole information is "hard data", and the simulations therefore always honour the information at the borehole positions.

5.3. Cognitive layer modelling

The cognitive layer model is developed as a framework model consisting of layers that are defined as the volume between surfaces. These surfaces are controlled by interpretation points defined in space and manually digitised and attached to cross sections, horizontal sections, boreholes, seismic sections, etc., according to the modeller's geological interpretations. Most interpretation points are attached to cross sections that were gradually moved through the model space and checked against perpendicular moveable cross sections. The interpretation points are instantaneously interpolated into surface grids providing an instant overview of the surface or boundary that is modelled. Erosional boundaries such as the bottoms of the buried valley and other type of boundaries were also modelled in this way. After construction, the exact delineations of the surfaces were refined by cutting along digitised region polygons and by applying a hierarchical system describing the internal stratigraphical order of the surfaces (as defined in the conceptual model, see Fig. 2). The hierarchical system ensures that e.g. two different chronostratigraphic surfaced do not cross. The older surface will be cut by the younger, so that surfaces cut each other according to the defined stratigraphical order. All volumetric units (as defined by surfaces) in the cognitive framework model were finally discretised into a regular voxel grid with a horizontal discretisation of 100 m × 100 m and a vertical discretisation 5 m.

6. Choice of 3D modelling methodologies

The geology in the area varies considerably with respect to the degree of complexity. The top layers of the outwash unit and Holocene appear laterally very uniform. The Palaeogene and Miocene layers are spatially also fairly uniform, even though they are occasionally interrupted by delta lobes, faults, erosional

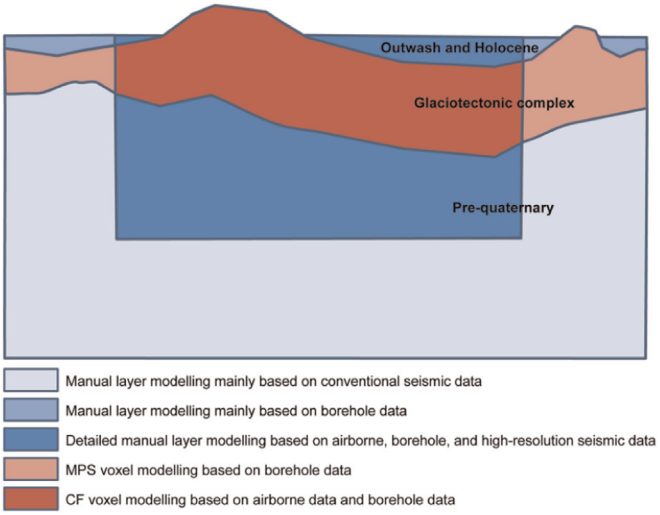

Fig. 5. Cross sectional, conceptual sketch showing how the different modelling techniques were applied with regard to geology and data availability.

surfaces and incising buried valleys. The buried valleys themselves have a higher degree of complexity, but are still composed by relatively big structures and infill units. The intensively deformed part of the section (the glaciotectonic complex) is much more spatially complex due to its composition of very small and detailed structures and because it includes layers of different origin mixed together. Prior to the 3D modelling process, it was considered that cognitive layer modelling would be the optimal choice for modelling everything but the glaciotectonic complex. But due to the high complexity of the glaciotectonics, it was considered far too time-consuming to create a reliable geological model within a reasonable timeframe. Other more automated methods were therefore considered to represent the internal structures of the complex in the model. Another factor to take into account when choosing the modelling method for the glaciotectonic complex was the difference in spatial data coverage. The glaciotectonic complex is split into two parts: one part inside and one part outside the area covered by SkyTEM and high-resolution seismics (Fig. 5). The CF modelling methodology was applied for the inside area, since this method is designed for modelling resistivity data in combination with borehole data. MPS was then applied outside and since we presume from our conceptual model that the origin and thus the shapes and internal structures are identical in the entire complex, it was decided to use the SkyTEM 3D resistivity grid (from the inside area) as training image for the area without resistivity data (outside area).

7. Model results

7.1. The CF model

For every voxel, the calculated clay fraction is given as a number between 0 and 100% clay. To incorporate this into the overall 3D model, the CF grid is converted into a discrete grid with 10% clay fraction intervals (see Fig. 6). The top of the CF model varies between ground level and down to depths of 40 m and the bottom reaches down to 140 m below sea level in some places. The main structures in the CF model generally resemble the structures in the SkyTEM resistivity grid so that areas with high resistivities show low clay content and areas with low resistivities show high clay content (Fig. 6). The CF model results show a high degree of

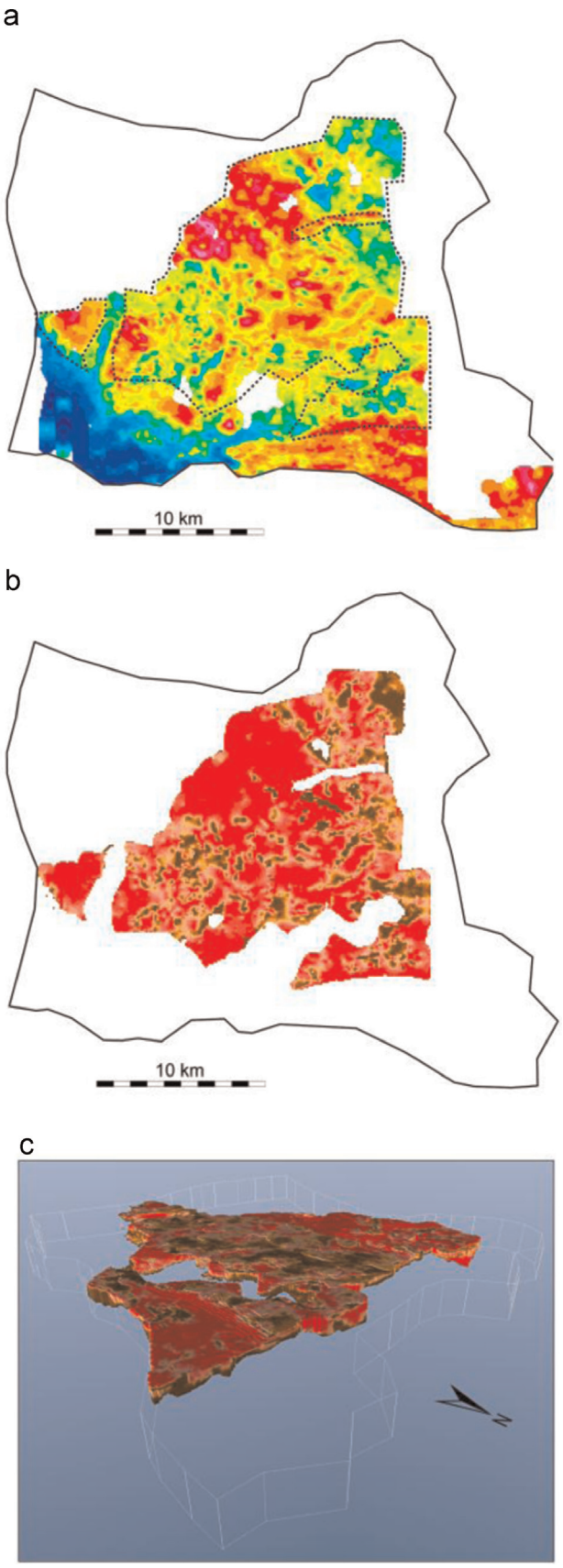

Fig. 6. Horizontal slice (7.5 m below sea level) through the resistivity grid (a) and through the resulting CF model (b). The extent of the final CF model is delineated by a hatched line on the resistivity map. 3D view of the CF model from northeast (c). See Fig. 9 for symbols and Fig. 3 for resistivity scale.

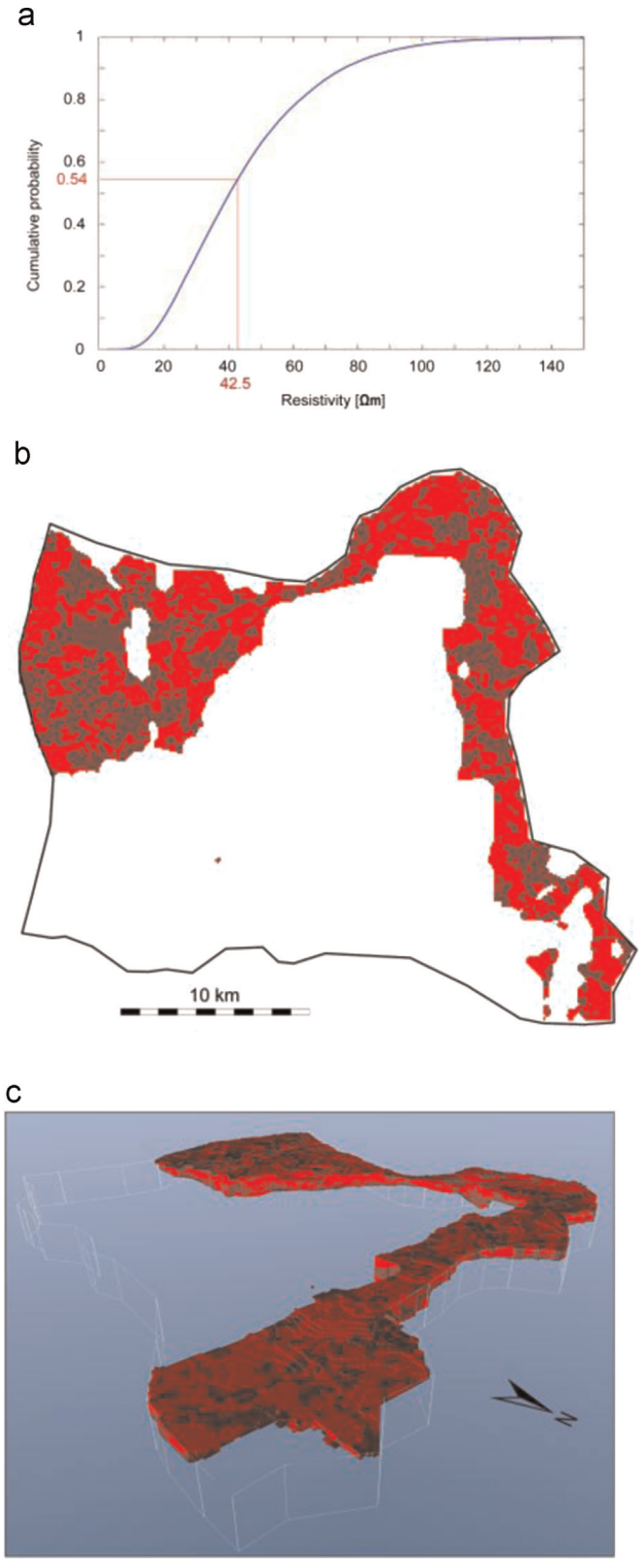

Fig. 7. (a) Cumulative probability distribution curve with the cut-off value reading (42.5 Ω m) used for the training image construction. (b) Horizontal slice through the resulting MPS model at 7.5 m below sea level. (c) 3D view of the MPS model from northeast. Red is sand, brown is clay; see legend in Fig. 9. (For interpretation of the references to colour in this figure legend, the reader is referred to the web version of this article.)

small-scale variations in the topmost 30 m. This is as expected since the resolution of the SkyTEM data is highest at shallow depths. Below this highly varying, but overall clayey interval, a 50–80 m thick unit of more or less clay-free deposits is present in most of the area. The clay-free interval here appears almost massive, and clayey structures are only randomly encountered within the unit. Below the clay-free interval, the CF model gradually shows higher clay content and the lower part is mainly composed of clay.

7.2. The MPS model

As noted above, the 3D resistivity grid is used as training image for the simulations. This is done by using the same methodology as in He et al. (2014b). The 3D resistivity data are translated into lithological information, in this case a binary model of sand or clay. The borehole data are used to calculate the clay content as a function of the depth, as well as the total clay content, which corresponds to 54%. The clay content (54%) is then employed to find the cut-off value used to divide sand and clay by reading the equivalent resistivity (42.5 Ω) on the cumulative probability distribution curve (Fig. 7). The training image is then created by counting all cells with resistivities below 42.5 Ω as clay and all cells with higher resistivities as sand. Finally, the MPS simulations are created by utilising the training image together with the hard information from the boreholes. The clay content in the simulations is derived from the function that describes the clay content with depth. A total of 100 simulations were made. Since the end purpose of our 3D model is groundwater flow modelling, we wanted a model with realistic structures and connectivity. We therefore selected one simulation, while accepting that this is just one possible solution. The simulation with the lowest RMSE between the simulated sand content and the sand content observed in the boreholes was selected as input to the 3D model.

The results of the simulation appear more heterogeneous and varied than the results of the CF modelling (Fig. 7). There is generally more clay in the MPS model than in the CF model, but the shapes of the structures resemble the ones in the CF model to some degree (compare Figs. 6, 7 and 11). The pattern appears more detailed with smaller structures than are seen in the CF result.

7.3. The cognitive layer model

The framework model (layer model) consists of 24 layer units and 32 surfaces representing layer boundaries and erosional unconformities (Fig. 8). The framework model also contains other surfaces like the decollement surface, sequence stratigraphic boundaries and top of pre-Quaternary. In accordance with the geology in the area, the cognitive layer model appears much more uniform and layered than the CF and MPS models. The continuity of the layers is, however, to some degree interrupted by the faults/flexures, erosional boundaries and the buried valleys.

7.4. The final combined model

After discretisation of the framework model into a voxel model and finalising of the automated modelling procedures, the resulting voxel models from each of the three sub-models were combined into one big voxel model covering the entire model area. The final combined voxel model consists of 302 rows, 335 columns and 168 layers thus totalling about 17 million voxels. The voxels are attributed with 37 lithological, lithofacies and lithostratigraphical units (Fig. 9). The model reaches down to a depth of 840 m, well below the Palaeogene and into the Limestone. The model therefore covers all layers with potential groundwater

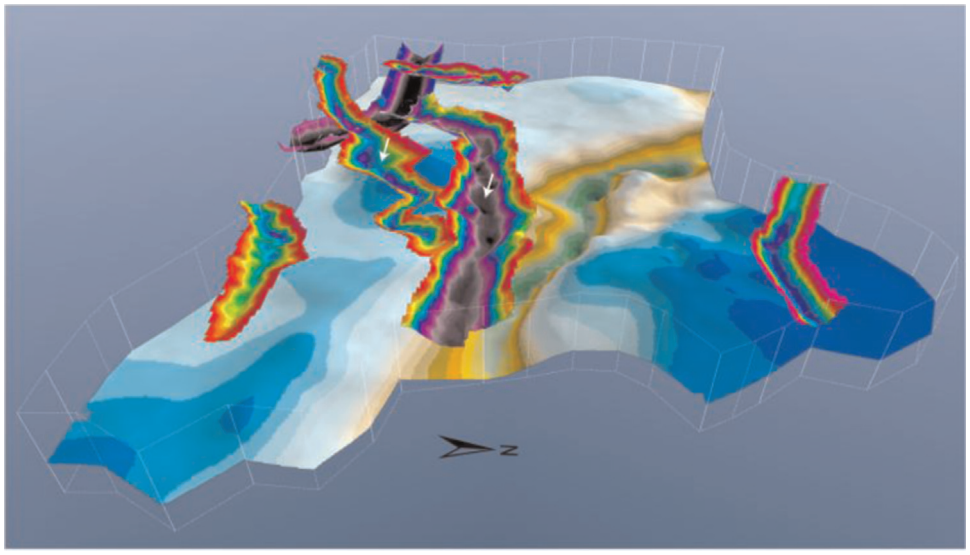

Fig. 8. 3D view of some of the surfaces in the framework model. Buried-valley surfaces (up to 470 m deep) are seen together with the surface of the deepest layer in the model – the Danian limestone (at 450–600 m depth). The Tønder Graben structure is clearly visible in this surface. The two arrows point to the two valleys outlined in Fig. 4. View angle: East to West.

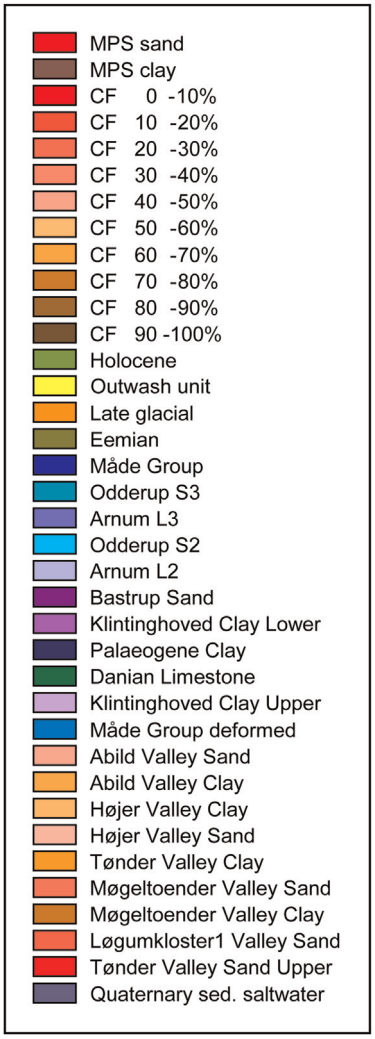

Fig. 9. Legend for voxel model units.

interest. Surfaces like the decollement surface, sequence stratigraphic boundaries, top of pre-Quaternary, etc., supplement the voxel model by crossing through the voxel volume.

The final voxel model without surfaces is shown in Figs. 10 and 11. The pre-Quaternary section is in the deepest part composed of the limestone followed by 150–200 m of marine Palaeogene clay. This deep section of the model is covered by the different Miocene formations composed of 100–300 m of marine and fluvial sand, silt and clay layers (Klintinghoved clay to Måde Group). The Miocene layers and the layers below are traversed by the Tønder Graben structure the central part of which is about 200 m deep. The Miocene is also frequently incised by the buried tunnel valleys (Fig. 8). Thick layers of both fine-grained and coarse-grained glaciofluvial material form the valley fill (Fig. 11). Compared to the manually constructed part of the model, the CF and the MPS models of the glaciotectonic complex appear much more detailed. The outwash deposits and the Holocene deposits are seen to cover the area except for the areas where the glaciotectonic complex is exposed as “hill-islands” above the outwash plain (Fig. 10).

8. Discussion

One of the major challenges encountered during the development of the 3D geological model in the area was to properly depict the internal structures of the glaciotectonic complex. Cognitive layer modelling was found to be appropriate for the undeformed parts of the model volume. This manual approach was possible because the geology is here composed of a relatively homogeneously layered succession that is generally well resolved by borehole and geophysical data. It was also possible to include the buried valleys in the cognitive layer model, even though the valleys have a somewhat complex architecture. We believe that the most accurate model is achieved by cognitive modelling when the geology is not too complex because expert background knowledge can be applied during the interpretation of the geophysical and the borehole data. Such background knowledge includes geological knowledge concerning the general stratigraphy of the area; knowledge about sequence stratigraphy, sedimentary and glacial

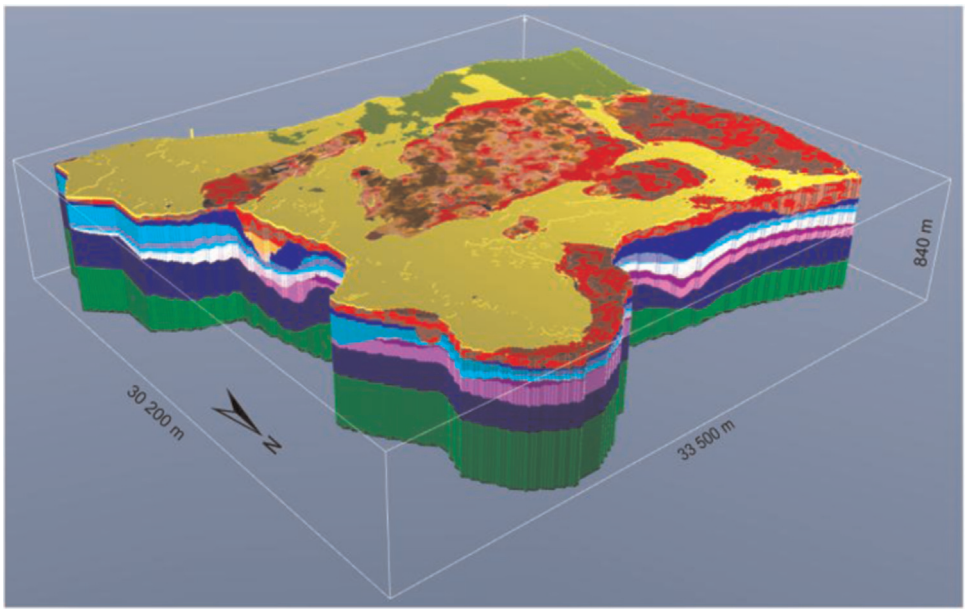

Fig. 10. 3D view (from the northeast) over the final voxel model. See Fig. 9 for legend. Vertical exaggeration 8 ×.

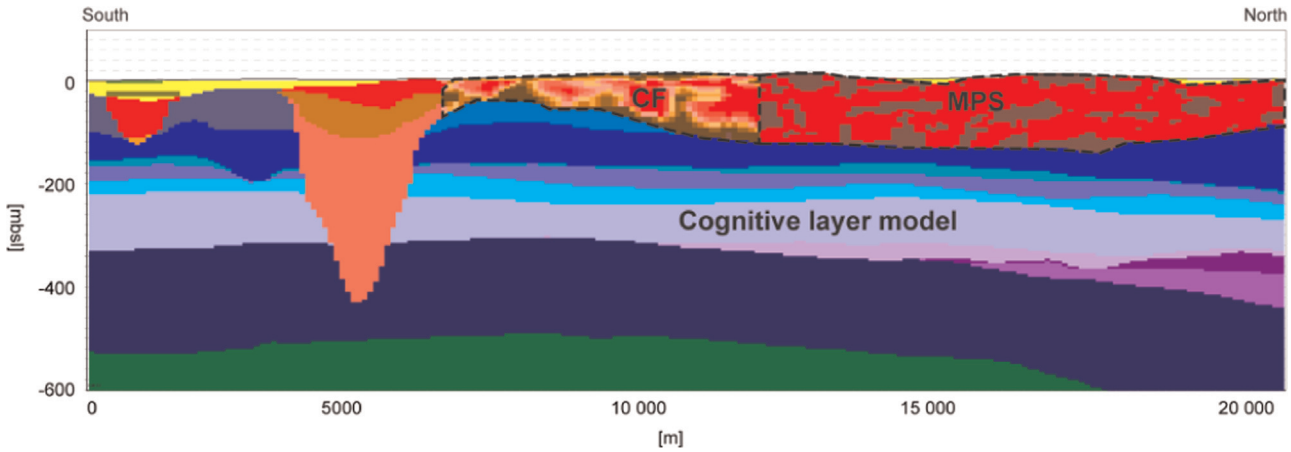

Fig. 11. S–N oriented cross section across the final voxel model. Vertical scale is in metres below sea level [mbsl] and the horizontal scale is in metres [m]. The three different origins of the model and the boundaries between them are indicated with text and dashed lines. Vertical exaggeration 8 ×. See Fig. 9 for legend.

processes; but also geophysical background knowledge enabling the modeller to take into account, e.g., the limitations of the data when resolving and map the geology (Jørgensen et al., 2013).

For the glaciotectonic complex, however, the cognitive manual modelling approach was not applicable. It was found to be too time-consuming to manually construct a 3D model of the very detailed and complex geology. Due to the low borehole and seismic data density, the delineation of the internal structures needs to rely almost entirely on the resistivity data. The CF method was therefore applied to efficiently produce a detailed clay fraction model of the glaciotectonic complex. Since the method only discriminates between sand and clay, it was not possible to further distinguish between different lithology types, e.g. Miocene clay and glaciolacustrine clay. According to the detailed seismic information and in line with the general expectation of how such a complex is typically composed (Aber and Ber, 2007), many of the small internal structures in the complex are not resolved in the model. This is most likely due to limitations in the resolution capability of the SkyTEM system (see also Høyer et al. (2013b)). The most detailed structures within the complex are therefore not captured and are thus represented in the CF model.

Another challenge encountered was the big differences in data density across the area. Where no dense SkyTEM data exist, it was not possible to resolve the structures of the glaciotectonic complex at all. Only the borehole data and poor conventional seismic data were available in these areas, and it was impossible to build the cognitive layer model for this part of the subsurface based on these data alone. Consequently, we chose to apply MPS for this area and then inform the model with structural information about the expected geology by applying the training image derived from the neighbouring SkyTEM data. The spatial distribution of sand/clay in the MPS simulation seems to some degree to resemble a glaciotectonic setting, but since the SkyTEM data only resolve the larger structures, the training image does not fully resemble the structures. This is especially significant for the deeper part of the complex where the resolution is poorer. A better resolution could possibly have been obtained if we have constructed the training image in other ways. It could, for instance, have been constructed from the neighbouring shallow seismic data (Liu et al., 2004) or perhaps from sketches of the expected structural composition of the complex (Huysmans and Dassargues, 2012; Liu et al., 2005).

When modelling techniques are to be chosen for a 3D

geological model project, parameters such as model purpose, geological complexity and available data types/data density should be considered and carefully taken into account. Depending on the situation at hand, some methods are more advantageous than others. Like in our model project, combinations of different methods within the model project may increase the quality of the model results and/or the time spent developing the model. It is, however, hardly an easy task to combine modelling methods within the same 3D model because the outcome of each method needs to be merged into the overall model. Since no software product can handle all the different methods, several software products must be brought into use when the combined modelling is conducted. This is often difficult because software products normally do not communicate very well. Another challenge is that experience and close collaboration are needed between a wide range of disciplines and experts, especially if geophysical data are involved.

9. Conclusion

We have developed a 3D geological model for an area with unevenly distributed data and with very different geological subdomains. Some subdomains are relatively homogeneously layered and others are very complex. These conditions call for the use of different modelling methods within the area. The choice of methods was guided by the conditions mentioned above, and the final model was composed of outcomes from (1) CF modelling applied within an area composed by a glaciotectonic complex and mapped by dense AEM data, (2) MPS modelling applied within the same complex but outside the area mapped by AEM data and, finally, (3) cognitive layer modelling applied in areas of the model volume where the geology is less complex and can thus be resembled manually on the basis of geophysical and/or borehole data. The final model was sampled into a voxel model combined with surfaces representing layer boundaries and erosional unconformities. Apart from pointing to solutions on how model methods can be combined, our study shows that it is advantageous to combine different modelling methods to increase model quality and to increase the efficiency of the modelling process.

Acknowledgements

The work was a part of a project collaboration between GEUS and The Danish Nature Agency. We are grateful to the two anonymous reviewers who helped improve the manuscript. Hans Guldager and Steen Thomsen are thanked for their support and helpful discussions. Rasmus Rønde Møller, Tom Martlev Pallesen, Anders Vest Christiansen and Torben O. Sonnenborg also contributed to the work. The data were partly collected as a part of the CLIWAT Project, which is co-funded by The Interreg IVB North Sea Region Programme, European Union (35-2-1-08).

References

Aber, J.S., Ber, A., 2007. Glaciotectonism. Elsevier, The Netherlands.
Andersen, L.T., 2004. The Fanø Bugt Glaciotectonic Thrust Fault Complex, Southeastern Danish North Sea. A study of large-scale glaciotectonics using high-resolution seismic data and numerical modelling. University of Aarhus, Geological Survey of Denmark and Greenland, Ministry of the Environment, Copenhagen, Denmark, p. 143, Report 2004/30.
Berg, C.B., Mathers, S.J., Kessler, H., Keefer, D.A., 2011. Synopsis of Current Three-dimansional Geological Mapping and Modeling in Geological Survey Organizations. Illinois State Geological Survey, Illinois.
Carle, S.F., Fogg, G.E., 1996. Transition probability-based indicator geostatistics. Math. Geol. 28, 453–476.
Christiansen, A.V., Foged, N., Auken, E., 2014. A concept for calculating accumulated clay thickness from borehole lithological logs and resistivity models for nitrate vulnerability assessment. J. Appl. Geophys. 108, 69–77.
Daly, C., Caers, J., 2010. Multi-point geostatistics-an introductory overview. First Break 28, 39–47.
Deutsch, C.V., Journel, A.G., 1998. GSLIB: Geostatistical Software Library and User's Guide, Second ed. Oxford University Press, Oxford.
Foged, N., Marker, P.A., Christiansen, A.V., Bauer-Gottwein, P., Jørgensen, F., Høyer, A.-S., Auken, E., 2014. Large scale 3d-modeling by integration of resistivity models and borehole data through inversion. Hydrol. Earth Syst. Sci. 18, 4349–4362.
Friborg, R., 1989. Geologisk model for Tønder, Nyhedsbrev Maj.
Friborg, R., Thomsen. S.,1999 . Kortlægning af Ribe Formationen. Et Fællesjysk Grundvandssamarbejde. Teknisk rapport Ribe Amt, Ringkjøbing Amt, Viborg Amt, Århus Amt, Vejle Amt, Sønderjyllands Amt.
GeoScene3D, 2014. ⟨http://www.geoscene3d.com⟩.
Gunnink, J., Siemon, B., 2014. Applying airborne electromagnetics in 3D stochastic geohydrological modelling for determining groundwater protection. Near Surf. Geophys. 13, 45–60.
Gunnink, J.L., Bosch, J.H.A., Siemon, B., Roth., B., Auken, E., 2012. Combining ground-based and airborne EM through Artificial Neural Networks for modelling glacial till under saline groundwater conditions. Hydrol. Earth Syst. Sci. 16, 3061–3074.
He, X., Koch, J., Sonnenborg, T.O., Jørgensen, F., Schamper, C., Refsgaard, J.C., 2014. Transition probability-based stochastic geological modeling using airborne geophysical data and borehole data. Water Resour. Res. 50, 3147–3169.
He, X., Sonnenborg, T.O., Jørgensen, F., Høyer, A.-S., Møller, R.R., Jensen, K.H., 2013. Analyzing the effects of geological and parameter uncertainty on prediction of groundwater head and travel time. Hydrol. Earth Syst. Sci. 17, 3245–3260.
He, X.L., Sonnenborg, T.O., Jørgensen, F., Jensen, K.H., 2014b. The effect of training image and secondary data integration with multiple-point geostatistics in groundwater modelling. Hydrol. Earth Syst. Sci. 18, 2943–2954.
Huysmans, M., Dassargues, A., 2012. Modeling the effect of clay drapes on pumping test response in a cross-bedded aquifer using multiple-point geostatistics. J. Hydrol. 450–451, 159–167.
Høyer, A.-S., Jørgensen, F., Foged, N., He, X., Christiansen, A.V., 2015. Three-dimensional geological modelling of AEM resistivity data-a comparison of three methods. J. Appl. Geophys. 115, 65–78.
Høyer, A.-S., Jørgensen, F., Piotrowski, J.A., Jakobsen, P.R., 2013a. Deeply rooted glaciotectonism in western Denmark: geological composition, structural characteristics and the origin of Varde hill-island. J. Quat. Sci. 28, 683–696.
Høyer, A.-S., Møller, I., Jørgensen, F., 2013b. Challenges in geophysical mapping of glaciotectonic structures. Geophysics 78, B284–B300.
Jørgensen, F., Møller, R.R., Nebel, L., Jensen, N.-P., Christiansen, A.V., Sandersen, P.B. E., 2013. A method for cognitive 3D geological voxel modelling of AEM data. Bull. Eng. Geol. Environ. 72, 421–432.
Jørgensen, F., Sandersen, P.B.E., 2006. Buried and open tunnel valleys in Denmark-erosion beneath multiple ice sheets. Quat. Sci. Rev. 25, 1339–1363.
Jørgensen, F., Scheer, W., Thomsen, S., Sonnenborg, T.O., Hinsby, K., Wiederhold, H., Schamper, C., Burschil, T., Roth, B., Kirsch, R., Auken, E., 2012. Transboundary geophysical mapping of geological elements and salinity distribution critical for the assessment of future sea water intrusion in response to sea level rise. Hydrol. Earth Syst. Sci. 16, 1845–1862.
Kessler, H., Mathers, S., Sobisch, H.G., 2009. The capture and dissemination of integrated 3D geospatial knowledge at the British Geological Survey using GSI3D software and methodology. Comput. Geosci. 35, 1311–1321.
Klimke, J., Wiederhold, H., Winsemann, J., Ertl, G., Elbracht, J., 2013. Three-dimensional mapping of Quaternary sediments improved by airborne electromagnetics in the case of the Quakenbrück Basin, Northern Germany. Z. Deutsch. Ges. Geowiss. 162, 369–384.
Koch, J., He, X., Jensen, K.H., Refsgaard, J.C., 2014. Challenges in conditioning a stochastic geological model of a heterogeneous glacial aquifer to a comprehensive soft data set. Hydrol. Earth Syst. Sci. 18, 2907–2923.
Liu, Y., Harding, A., Abriel, W., Strebelle, S., 2004. Multiple-point simulation integrating wells, three-dimensional seismic data, and geology. AAPG Bull. 88, 905–921.
Liu, Y., Harding, A., Gilbert, R., Journel, A.G., 2005. A Workflow for Multiple-point Geostatistical Simulation. In: Leuangthong, O., Deutsch, C.V. (Eds.), Geostatistics Banff 2004, Quantitative Geology and Geostatistics. Springer, Netherlands, pp. 245–254.
Orbicon, 2010. Miljøcenter Ribe Boringsundersøgelse DGU Nr. 167.1538. Unpublished report.
Orbicon, 2011. Naturstyrelsen Ribe Boringsundersøgelse DGU Nr. 167.1545. Unpublished report.
Raiber, M., White, P.A., Daughney, C.J., Tschritter, C., Davidson, P., Bainbridge, S.E., 2012. Three-dimensional geological modelling and multivariate statistical analysis of water chemistry data to analyse and visualise aquifer structure and groundwater composition in the Wairau Plain, Marlborough District, New Zealand. J. Hydrol. 436, 13–34.
Rambøll, 2010. Seismisk kortlægning ved Tønder. Unpublished report.
Rasmussen, E.S., Dybkjær, K., Piasecki, S., 2010. Lithostratigraphy of the upper Oligocene – Miocene session in Denmark. Geol. Surv. Denmark Greenl. Bull. 22, 93.
Remy, N., Boucher, A., Wu, J., 2009. Applied Geostatistics with SGeMS, Cambridge University Press, Cambridge, UK, 286 pp.
Royse, K.R., 2010. Combining numerical and cognitive 3D modelling approaches in order to determine the structure of the Chalk in the London Basin. Comput.

Geosci. 36, 500–511.
Schamper, C., Auken, E., Sørensen, K.I., 2014a. Coil response inversion for very early time modelling of helicopter-borne time-domain electromagnetic data and mapping of nearsurface geological layers. Geophys. Prospect. 62, 658–674.
Schamper, C., Jørgensen, F., Auken, E., Effersø, F., 2014b. Assessment of near-surface mapping capabilities by airborne transient electromagnetic data – an extensive comparison to conventional borehole data. Geophysics 79, B187–B199.
Sharpe, D., Russell, H.A.J., Logan, C., 2007. A regional 3-dimensional geological model of the Oak Ridges Moraine area, Ontario, Canada. J. Maps 2007, 239–253.
Stafleu, J., Maljers, D., Gunnink, J.L., Menkovic, A., Busschers, F.S., 2011. 3D modelling of the shallow subsurface of Zeeland, the Netherlands. Neth. J. Geosci. Geol. Mijnb. 90, 293–310.
Steuer, A., Siemon, B., Auken, E., 2009. A comparison of helicopter-borne electromagnetics in frequency- and time-domain at the Cuxhaven valley in Northern Germany. J. Appl. Geophys. 67, 194–205.
Strebelle, S.B., 2002. Conditional simulation of complex geological structures using multiple-point statistics. Math. Geol. 34, 1–21.
Sørensen, K.I., Auken, E., 2004. SkyTEM-A new high-resolution helicopter transient electromagnetic system. Explor. Geophys. 35, 191–199.
Thomsen, S., 1991. Kortlægning af dybe gru ndvandsmagasiner, 1. statusrapport, p. 30.
Venteris, E.R., 2007. Three-dimensional modeling of glacial sediments using public water-well data records: an integration of interpretive and geostatistical approaches. Geosphere 3, 456–468.
Viezzoli, A., Auken, E., Munday, T., 2009. Spatially constrained inversion for quasi 3D modelling of airborne electromagnetic data-an application for environmental assessment in the Lower Murray Region of South Australia. Explor. Geophys., 40.
Wycisk, P., Hubert, T., Gossel, W., Neumann, C., 2009. High-resolution 3D spatial modelling of complex geological structures for an environmental risk assessment of abundant mining and industrial megasites. Comput. Geosci. 35, 165–182.